Applied Surface Science 331 (2015) 98–107

Contents lists available at ScienceDirect

Applied Surface Science

journal homepage: www.elsevier.com/locate/apsusc

Sol–gel synthesis of photoactive kaolinite-titania: Effect of the preparation method and their photocatalytic properties

Godlisten N. Shao[a,c], Marion Engole[b], S.M. Imran[a], Sun Jeong Jeon[a], Hee Taik Kim[a,*]

[a] Department of Chemical Engineering, Hanyang University, 1271 Sa 3-dong, Sangnok-gu, Ansan-si, Gyeonggi-do 426-791, Republic of Korea
[b] Department of Water Resources Engineering, Busitema University, Tororo, Uganda
[c] Department of Chemistry, Mkwawa College, University of Dar es Salaam, Iringa, United Republic of Tanzania

ARTICLE INFO

Article history:
Received 3 September 2014
Received in revised form
15 December 2014
Accepted 31 December 2014
Available online 12 January 2015

Keywords:
Sol–gel process
Kaolinite-titania
Heterogeneous catalysis
Calcination
$TiOCl_2$

ABSTRACT

Supporting TiO_2 on different materials is a potential strategy to improve the photochemical properties of the resulting composites. Kaolinite (K) was used as a support to synthesize a series of kaolinite-titania (K-TiO_2) photocatalysts with desirable properties for decolorization of organic contaminants. Initially, TiO_2 sol was formed through gelation of titanium oxychloride using ammonium hydroxide solution and subsequent peptization of the preformed gel in a low concentration of nitric acid. The sol was reacted with different concentrations of kaolinite at different pH conditions to yield K-TiO_2 composites with different TiO_2 compositions. The physicochemical properties of the photocatalysts were examined by XRD, FTIR, TGA, SEM-EDAX, XRF, UV–visible DRS, TEM and nitrogen gas physisorption studies analyses. XRD results revealed that through varying pH of the reaction a mixture of TiO_2 crystals can be attained in the sintered samples. A simple photocatalytic experiment of the calcined photocatalysts was carried out to evaluate the decolorization of methylene blue in the presence of an artificial UV source. The obtained results were exquisitely compared to those of the ZrO_2-TiO_2 based composites obtained in our previous study. It was revealed that the amount of TiO_2 in the composites and the calcination temperature had a profound effect on the microstructure and photocatalytic performance of the samples. Thus, the KT34-600 sample exhibited the highest activity of all due to its superior properties. This study provides a criterion for selection of precursors, synthetic routes and support suitable for the formation of metal oxides composites with desirable properties for heterogeneous catalysis.

© 2015 Elsevier B.V. All rights reserved.

1. Introduction

Since the breakthrough of the photocatalytic splitting of water on TiO_2 by Fujishima and Honda in 1972, there have been incredible efforts to improve the physicochemical properties and applications of semiconductors [1–4]. Recently, heterogeneous catalysis by semiconductors has attracted many researchers due to its promising effectiveness in degrading toxic pollutants for environmental cleanup and water purification. TiO_2 is a chemically inert, non-toxic, highly oxidative and cost-effective metal oxide; vital attributes for heterogeneous catalysis and solar energy conversion materials [1–8]. Therefore, various metal oxide semiconductors such as TiO_2, SiO_2-TiO_2 and ZrO_2-TiO_2 have been widely used due to their unique optical and electronic properties [9–11]. Meanwhile, the rapid increase of population and industrial pollution entails large-scale industrial production of heterogeneous photocatalysts to reduce toxic pollutants and improve the availability of clean water. Thus, the formulation of facile and controllable synthetic approaches and consumption of less expensive sources are required to boost large-scale industrial production and commercialization of heterogeneous catalysts.

To date, metal oxide incorporated TiO_2 nanoparticles suitable for heterogeneous catalysis has been extensively reported [12–16]. In order to yield photocatalysts with desired properties for these applications, several vital properties related to purity, porosity, surface area, aggregation and crystallinity should be considered. These properties preferably affect the application of the final product and are largely dependent on the synthetic approach and precursors. During synthesis of TiO_2 based semiconductors using Ti (IV) alkoxides as a TiO_2 sources, tedious and complicated synthetic methods are involved. In most reports, tetrabutylorthotitanate and titanium (IV) tetraisopropoxide are typically consumed as TiO_2 sources and perhaps surfactants or organic solvents are used to improve the pore structure of the final product [17–19]. These precursors are understandably expensive and hazardous hampering large-scale

* Corresponding author. Tel.: +82 31 400 5274; fax: +82 31 419 7203.
E-mail addresses: shaogod@gmail.com (G.N. Shao), khtaik@hanyang.ac.kr, khtaik@yahoo.com (H.T. Kim).

http://dx.doi.org/10.1016/j.apsusc.2014.12.199
0169-4332/© 2015 Elsevier B.V. All rights reserved.

industrial production and commercialization of photocatalysts. Thus, the possibility of consuming less expensive precursors and simplified synthetic routes would suit production of metal oxide semiconductors for numerous applications.

Meanwhile, kaolinite ($Al_2O_7Si_2{\cdot}2H_2O$) is a cheap and non-toxic naturally occurring layered aluminosilicate inorganic polymer widely used in the paper industry [20–22]. Indeed, the chemical structure (especially the presence of the reactive hydroxyl groups) of kaolinite influences many chemical and ion exchange reactions [23,24]. Therefore, it can be considered as an excellent substrate for anchoring metal oxides to form nanocomposites for a myriad of applications [25,26]. K-TiO_2 nanocomposite has extensively been reported owing to its ease of synthesis and it is an environmentally benign process. Various TiO_2 precursors such as $TiCl_4$, $TiOSO_4$ and Ti (IV) alkoxides have been used in the preparation process of K-TiO_2 [9,14,25–27]. Even though $TiCl_4$ is still a cost-effective precursor, its volatility and the dimerization behavior that occurs during the synthesis process make this precursor difficult to handle.

Our research group has been providing a sequel clarifying the use of $TiOCl_2$ solution (rarely reported TiO_2 precursor) to fabricate various photocatalysts with desirable properties for degradation of organic contaminants [10–12,28–30]. Using $TiOCl_2$ solution as a TiO_2 precursor yields a homogeneous product with even distribution of primary particles and high TiO_2 loadings. Indeed, it is a rarely reported TiO_2 source but it is a precursor of great importance since it allows the formation of TiO_2 materials at ambient conditions and on a large-scale [11,12,28,31]. It is thought that the use of $TiOCl_2$ as a TiO_2 precursor and the synthetic route used to synthesize TiO_2 both influence the physicochemical properties of the final product. For instance, in our previous study we found that abnormal grain growth can occur in ZrO_2-TiO_2 microstructures depending on the Ti-to-Zr ratio and calcination temperature [10]. Thus, the synthesis of various TiO_2 based composites using $TiOCl_2$ would increasingly provide flexibility in the production of diverse materials with desirable properties for numerous industrial applications.

The present study proposes a controllable and reproducible approach to produce K-TiO_2 photocatalysts with a mixture of TiO_2 crystals and improved photochemical performance using titanium oxychloride as a TiO_2 precursor. The influence of pH and TiO_2 content on the microstructure of the K-TiO_2 photocatalysts was exquisitely investigated. Moreover, the photocatalytic properties of the obtained photocatalysts were tested in the photodecolorization of methylene blue solution to substantiate their practical reliability in degrading non-biodegradable toxic pollutants.

2. Experimental procedure

2.1. Materials

$TiOCl_2$ (25 wt.%) was procured from Kukdong Chemicals Co. Ltd., South Korea while ammonium hydroxide solution (28%) was bought from Dae-Jung Chemical and Metal Co. Ltd., South Korea. Kaolinite ($Al_2O_7Si_2{\cdot}2H_2O$), Methylene blue hydrate and 60% HNO_3 were purchased from Sigma–Aldrich. These chemical reagents were used as acquired from their commercial sources without further purification.

2.2. Synthesis process

In a typical experiment, 1.6 g kaolinite was added into 100 mL of deionized (DI) water and the suspension stirred at a temperature of 50 °C for 2 h (**solution A**). TiO_2 sol (**solution B**) was promptly prepared by the same procedures outlined in our previous report but with some modifications [32]. Concisely, 10 mL of $TiOCl_2$ solution and 60 mL of DI water was stirred for 1 h followed by gelation through drop-wise addition of ammonium hydroxide to obtain a solid gel. The gel was then peptized in 30 mL, 0.02 M nitric acid under vigorous stirring to obtain a TiO_2 sol which was further stirred at room temperature for 1 h. Solution B was then added drop-wise into solution A under vigorous stirring. The K-TiO_2 suspension was further stirred at 50 °C for 1 h.

After 1 h, the suspension was divided into two portions in order to prepare two different slurries at pH 4 and 8 through adjusting pH with ammonium hydroxide solution. These slurries were then aged at 80 °C for 6 h, filtered off and washed with water and then dried at 120 °C for 6 h. The dried powders were thermally treated in a box furnace at temperatures ranging from 400 to 900 °C for 2 h in an air atmosphere. The raw samples were named KT1*X* (for the K-TiO_2 sample obtained when 1.6 g of kaolinite was used; *X* is the final pH of the slurry). The calcined samples were dubbed KT1*X*-calcination temperature. For example, the sample obtained at pH 8 and calcined at 900 °C was dubbed KT18-900. The same experimental procedures were followed through varying the feeding weight of kaolinite to 0.8, 0.4 and 0.2 g in order to obtain KT2*X*, KT3*X* and KT4*X* series, respectively. For the sake of comparison pure TiO_2 powder (TT00) was synthesized according to procedures outlined in reference [10]. Briefly, the TiO_2 sol obtained after peptization was stirred at room temperature for 2 h. The pH of the sol was adjusted to 6 and the obtained slurry was aged at a temperature of 80 °C for 4 h under constant stirring. The product was collected by filtration and dried at 100 °C for 6 h and labeled TT (for pure titania); the samples calcined at 400 and 600 °C were expressed as TT400 and TT600, respectively.

2.3. Photodegradation experiment

The photodecolorization experiments of methylene blue (MB) solutions were carried out to evaluate the practical reliability of the composites yielded. A glass reactor equipped with a 100 W high-pressure mercury lamp (UM-103B-B USHIO Japan) was used and the temperature of the solution maintained at 25 °C throughout the experiment. Briefly, 200 mL of a 32 mg/L MB solution was placed in the reactor followed by the addition of 0.6 g/L of the photocatalyst (calculated depending on the amount of TiO_2 in the sample as was estimated by XRF). Firstly, the solution was magnetically stirred in darkness to determine the adsorption amounts of the samples. After the first step, the suspension was irradiated under a UV light source as a function of irradiation time under constant stirring. During this process samples were regularly withdrawn from the reactor, centrifuged (Heraeus Pico 17 Centrifuge-Thermo Scientific, Germany) and the supernatants analyzed using a UV–vis spectrometer. The photocatalytic decolorization of MB was expressed as a function of the relative concentration of MB solution (C/C_o) at a characteristic absorption of MB at 660 nm with reaction time; where C_o is the initial concentration and C is the concentration of MB solution at an absorption of MB at 660 nm at time, t. Since $\mathrm{Ln}\, C_o/C = kt$, a linear relationship between the logarithm of relative concentration of MB ($\mathrm{Ln}\, C_o/C$) with the irradiation time was used to estimate the decolorization rate constants (k) by the photocatalysts used for photocatalytic reactions [10,11,33].

2.4. Characterization

The infrared spectra of the representative samples were recorded by FTIR Spectrometry (Avatar 360 E.S.P, Nicolet). The IR spectrometer was equipped with a DTGS KB detector to measure the transmittance of the KBr pellets containing 2 wt.% of the sample. An average of 64 scans with a wave number resolution of 4 cm^{-1} and optical velocity of 0.6334 cm^{-1} was collected from 400 to 4000 cm^{-1}. The elemental content of the samples was determined by an X-Ray fluorescence Spectrometer (XRF; XRF-1700,

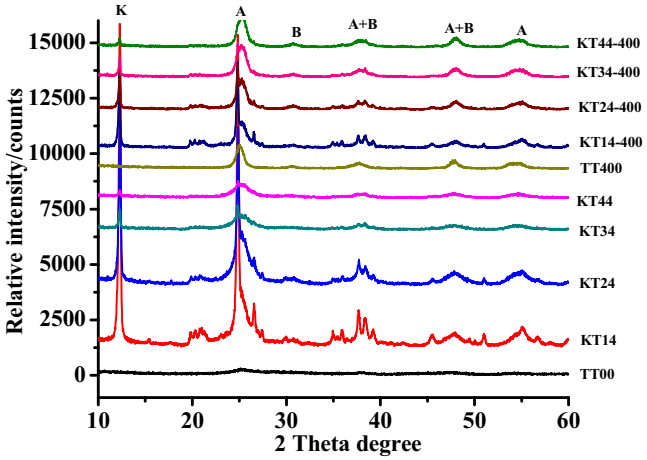


Fig. 1. XRD of raw and calcined pure TiO_2, raw samples of K-TiO_2, K-TiO_2 photocatalysts obtained at pH 4 and calcined at 400 °C. K represents the principal peak of kaolinite while B = brookite and A = anatase TiO_2.

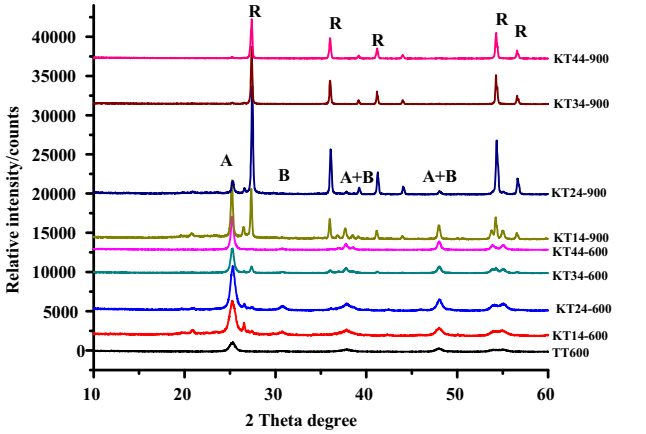


Fig. 2. XRD of pure TiO_2 calcined at 600 °C; K-TiO_2 photocatalysts obtained at pH 4 and calcined at 600 °C and 900 °C. B = brookite, A = anatase and R = rutile TiO_2.

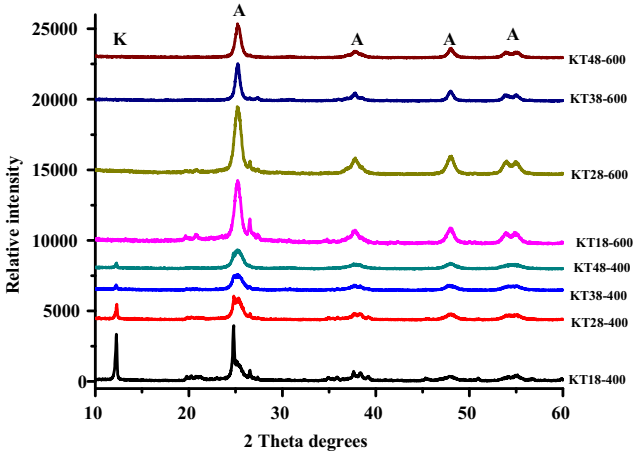


Fig. 3. XRD of K-TiO_2 photocatalysts obtained at pH 8 and calcined at different calcination temperatures. K represents the principal peak of kaolinite while A = anatase TiO_2.

Shimadzu Co., Japan with a detection limit of 10 ppm and depth resolution up to 10 μm). ZAF corrections (atomic number, *Z*) were used to determine the molar ratios of the elements present in the samples. An X-ray Diffractometer (XRD-6000, Shimadzu) was used to record the X-ray diffractograms of the samples. The accelerating voltage and applied current were 40 kV and 100 mA, respectively. The Scherer's equation [34] was used to estimate the crystallite size of the powders. A nitrogen gas adsorption–desorption instrument (Micrometrics ASAP 2020) was used to study the Brunauer–Emmett–Teller (BET) surface area and the porosity measurements of the raw and calcined samples. All the samples examined were degassed at 200 °C for 2 h prior to actual measurements.

Thermogravimetric analysis (TGA) and differential TGA were carried out using a differential thermal-thermogravimetric analyzer (DT-TG 7300, SEIKO INST-Japan) and TGA, TA Instruments, Q500, USA. It was performed in nitrogen gas at a heating rate of 10 °C/min from room temperature to 1000 °C. The Field emission scanning electron microscopy (FE-SEM, Hitachi S-4800, Japan) was used to study the morphology of the samples obtained at different conditions. The FE-SEM was coupled with energy dispersive spectroscopy (EDS) to assess the elemental composition of the powders synthesized via this method. X-ray mapping images were also collected during SEM analysis. Transmission electron microscopy (TEM, Jeol JEM 2100F, Korea) was employed to study the distribution and size of the particles. The diffuse reflectance Spectra (DRS) of the samples was recorded by a UV–vis Spectrophometer (Shimadzu, UV-2600) using $BaSO_4$ as a reference in the region from 200 to 900 nm. A UV–vis Spectrometer (Optizen 2021 UV, Korea) was used to acquire the absorption spectra.

3. Results and discussion

3.1. Crystal structure

The powder XRD analysis was essentially performed to investigate the phase structure and crystallite size of the samples. The XRD patterns of raw and calcined K-TiO_2 samples with different TiO_2 content and obtained at pH 4 are presented in Figs. 1 and 2 while the diffractograms of the samples obtained at pH 8 and sintered at the calcination temperatures of 400 °C and 600 °C are compiled in Fig. 3. All samples obtained at different pH conditions and calcined at different calcination temperatures showed different XRD patterns. Fig. 1 shows that raw TiO_2 was amorphous indicating that the sample was mainly composed of titanium hydroxides but the peaks assignable to anatase TiO_2 crystals were observed in the sample calcined at 400 °C. All of the as-prepared K-TiO_2 samples obtained at different conditions retained the sharp peak of K (0 0 1) at $2\theta = 12.3°$. Nevertheless, the intensity of the K (0 0 1) was essentially dependent on the amount of the TiO_2 present in the sample. In the samples with low amount of TiO_2 (KT1 and KT2) a sharp peak with high intensity can be observed while this peak is diminished in the samples with higher amount of the TiO_2 (KT3 and KT4).

A decrease of the sharp K (0 0 1) and K (0 0 2) peaks in the K-TiO_2 samples sintered at the calcination temperature of 400 °C was noticed. The decrease of the kaolinite peaks is attributable to either the intercalation or adsorption of Ti-polycations on the surface of kaolinite [14,27]. This implies that the presence of the kaolinite peaks in the samples depends both on the sintering temperature and TiO_2 content. Also, the samples calcined at 400 °C revealed the presence of brookite and anatase TiO_2 crystals. These TiO_2 polymorphs were retained even after calcining the samples at 600 °C (Fig. 2). Samples calcined at 900 °C reveal that the brookite and anatase peaks observed in the KT14-600 and KT24-600 underwent partially anatase-to-rutile transformation (ART) or brookite-to-rutile phase transformation (BRT). A complete ART and BRT can be observed in the KT34-900 and KT44-900 samples. The partial phase transformation registered in KT14-900 and KT24-900 samples is due to the presence of high kaolinite content (≥33%) which

Table 1
Grain size of different TiO_2 particle obtained at different conditions.

Calcination temp. (°C)	Phase	Sample name and crystallite size (nm)							
		KT14	KT18	KT24	KT28	KT34	KT38	KT44	KT48
600	Anatase	14.6	11.6	12.8	12.0	19.2	16.0	22.8	13.4
	Brookite	16.7	–	30.6	–	28.3	–	27.7	–
900	Anatase	26.7	29.2	38.0	31.2	–	–	–	–
	Rutile	91.7	92.3	42.1	42.8	47.2	42.1	40.4	39.4

suppressed the ART or BRT i.e. similar results have customarily been reported elsewhere [11,13,28,32].

Fig. 3 shows the XRD diffractograms of the representative samples of the K-TiO_2 obtained at pH 8 and calcined at different temperatures. A thorough comparison of the diffractograms of the samples synthesized at pH 4 and pH 8 demonstrates appealing results. It can be noticed that the brookite peaks observed in the samples synthesized at pH 4 and calcined at calcination temperatures ≤600 °C are absent in the sintered samples obtained at pH 8. Thus, only the anatase TiO_2 crystals formed in the K-TiO_2 systems obtained at pH 8 and calcined at calcination temperatures ≤600 °C. This implies that the phase structure of K-TiO_2 materials depends on the calcination temperature, synthetic conditions and the amount of the TiO_2 present in the composite. Hence, the optimization of these parameters is very fundamental during synthesis of the composites with desirable physicochemical properties.

The effect of sintering on the microstructure of the K-TiO_2 photocatalysts reported by Wang et al. [35] revealed that the presence of kaolinite facilitates the formation of anatase and prevents the ART. However, findings of the present study are different from those reported by Wang et al. demonstrating that the formation of the TiO_2 crystals in the K-TiO_2 materials can be influenced by several factors. Meanwhile, the TiO_2 products with mixed phase exhibit higher photocatalytic performance than single phase [14]. It was formerly reported [36–38] that a TiO_2 semiconductor with a mixed phase can be synthesized through thermolysis of titanium halides in strong acids. Zhang et al. [14] introduced a convenient approach for the preparation of K-TiO_2 materials with a mixed phase. It was found that the formation of different TiO_2 crystals depends on the drying and calcination temperatures of the resulting samples. It is thought that under favorable conditions such as acidity and temperature, the presence of ligands from strong acids facilitates the formation of Ti^{4+} monomers that can rearrange during polymerization to form different phases [36,37]. In the present study, K-TiO_2 composites were synthesized through reacting kaolinite and TiO_2 sol at pH 4 and 8 and subsequent calcination of the obtained powders. Since the mixed phases were attained in the calcined samples prepared at pH 4, it can presumably be thought that the sintering temperature facilitated the formation of the different TiO_2 crystals through rearrangement of the TiO_6 octahedral during polymerization and the crystal growth process [13,28].

The grain size of samples was estimated by the Scherrer equation [34] and the results are summarized in Table 1. The grain size of the anatase in samples calcined at 600 °C was between ~12 and 23 nm whereas brookite registered particle size ranging from ~17 to 31 nm. The grain size of the anatase TiO_2 crystals was significantly increased to ~27–38 nm upon increasing the calcination temperature to 900 °C. It can be noticed that the particle size of the rutile obtained after ART or BRT were larger (40–92 nm) than those of either anatase or brookite. It is well known that rutile is the most thermodynamically stable phase of TiO_2; therefore calcination at higher temperatures facilitated grain growth and ART [13,28]. Consequently, the coexistence of anatase and rutile in the KT14-900 and KT24-900 samples showed

Table 2
XRF composition of kaolinite-titania composites obtained at different conditions.

Sample name	Amount of oxides (%)			
	TiO_2	SiO_2	Al_2O_3	K_2O
Kaolinite	–	55.17	42.05	2.78
KT18-400	42.71	29.79	26.24	1.26
KT28-400	67.26	16.87	15.15	0.72
KT38-400	81.22	9.64	8.74	0.40
KT48-400	89.13	5.68	4.97	0.22

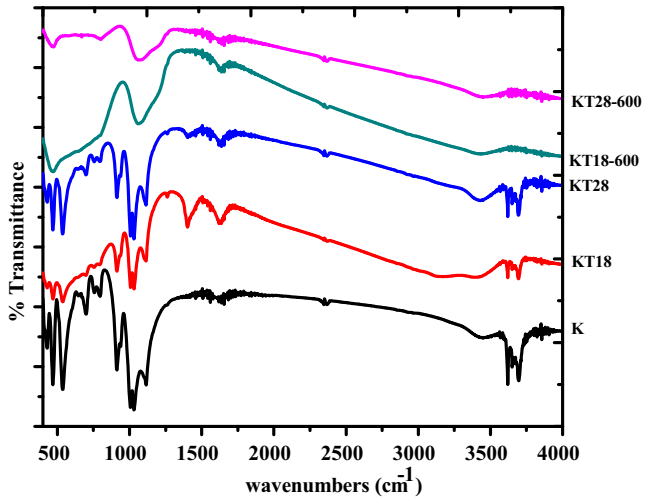


Fig. 4. FTIR spectra of pure kaolinite, as-synthesized and calcined samples of K-TiO_2 composites.

that phase transformation is dependent on the particle size, TiO_2 content and the sintering temperatures. The grain size of rutile was <93 nm indicating that these materials are thermally stable and can be suitable for different applications [39].

3.2. XRF and FTIR analyses

Initially, the elemental content of pure kaolinite and K-TiO_2 samples obtained at pH 8 and calcined at 600 °C were determined by XRF and the results are presented in Table 2. Pure kaolinite used in the present study contained K_2O, SiO_2, and Al_2O_3 metal oxides. Through varying the feeding amount of kaolinite during synthesis of K-TiO_2, photocatalysts with kaolinite content <42% were yielded. Fig. 4 shows the FTIR spectra of pure kaolinite, raw and calcined powders of K-TiO_2 obtained at pH 8. The IR spectra of the as-synthesized KT18 and KT28 samples showed vibrations similar to those displayed by pure K. The stretching and bending vibrations of the O–H groups of the water adsorbed in the samples can be seen at ~3440 cm^{-1} and 1635 cm^{-1}, respectively. The vibration bands of Si–OH and Si–O can be seen at 1110, 1020, 802 cm^{-1} and 470 cm^{-1}. The bands at 3600–3720 cm^{-1} and 920 cm^{-1} are attributable to the vibration of inner and outer Al–OH bonds [27,35]. The peaks corresponding to the Si–O–Al heterolinkage are observed at 750, 700 and

Table 3
Surface area, pore diameter and pore volume distribution of the samples obtained at pH 8.

Sample name	Surface area (m^2/g)	Pore volume (cm^3/g)	Pore size (nm)
TT00	328	0.27	3.1
K	8	0.03	28
KT18	169	0.12	4.1
KT28	259	0.13	3.7
KT38	265	0.12	3.4
KT48	320	0.13	3.3
TT600	88	0.15	4.8
KT18-600	47	0.10	3.7
KT28-600	73	0.15	5.7
KT38-600	52	0.12	6.7
KT48-600	71	0.13	5.4

540 cm^{-1}. The IR spectra of the KT18-600 and KT28-600 depict the substantial disappearance of vibration bands assignable to Al–OH. However, there is the formation of a broad peak between 920 cm^{-1} and 1280 cm^{-1} as a result of the superposition of Ti–O, Si–O and Al–O. It can also be seen that the stretching vibration of Ti–O and Si–O from 450 to 900 cm^{-1} masked the peaks for the symmetrical vibration of Si–O–Si and Si–O–Al which appear at 540–780 cm^{-1} [35]. Calcination of samples at higher temperatures facilitated the subsequent condensation of –OH groups from Si–OH and Ti–OH to form Si–O–Si, Ti–O–Si and Ti–O–Ti linkages and therefore the intensities of –OH at 1630 cm^{-1} and 3440 cm^{-1} were decreased [35]. It was formerly reported [40] that during calcination the disordering of the kaolinite structure occurs as a results of loosing –OH groups. This leads to the disappearance of the peaks between 1000 cm^{-1} and 1250 cm^{-1} and therefore a shoulder appears at ~1200 cm^{-1} as can be noticed in the IR results of the present study. XRD results showed that the crystallinity of TiO_2 increased with increasing calcination temperatures with consequent disappearance of the sharp kaolinite peaks. This indicates that during thermal treatment, the interaction between kaolinite and TiO_2 can be enhanced through kaolinite dehydroxylation and polymerization of TiO_2 [31,40].

3.3. UV–vis diffuse reflectance spectroscopy

The UV–Visible Diffuse Reflectance Spectra (UV–vis DRS) of the samples yielded in this process was examined and the results are presented in Fig. 5. Fig. 5A shows the UV–vis DRS spectra of pure TiO_2 and K-TiO_2 samples while Fig. 5B demonstrates a Tauc's plot used for the estimation of the band gaps of the samples. All spectra of the composite materials revealed a blue shift to higher energy regions compared to pure and calcined TiO_2. However, the absorption edge of all samples was below 400 nm. The results of the present study are quite similar to those reported by Zhang et al. [14] signifying that the addition of kaolinite in TiO_2 yields composites with superior optical properties. Therefore, these composites will have improved photocatalytic performances as a result of the formation of materials with improved redox ability. Moreover, the Tauc's plot in Fig. 5B shows that the band gaps of all samples are centered between 3.0 and 3.2 eV.

3.4. Nitrogen gas physisorption studies

The textural characteristics of the as-prepared and calcined samples were investigated by the nitrogen gas adsorption–desorption method at 77 K. A summary of the BET surface areas, pore volumes, and pore sizes for these samples are given in Table 3. The surface area of both raw and calcined composites was expectedly larger than that of pure kaolinite but smaller than that of pure TiO_2. The highest surface area in the composites was registered in the KT48 sample (320 m^2/g) that is very close to that of pure TiO_2 (327 m^2/g). The BET surface areas of the

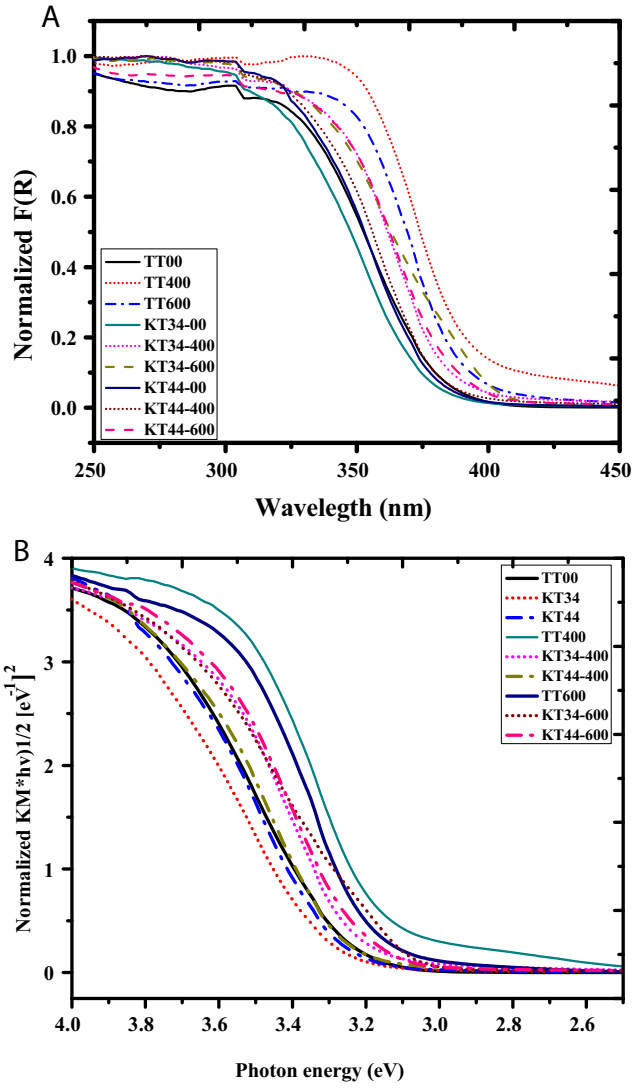


Fig. 5. UV–vis diffuse reflectance spectra of different photocatalysts (A) and their corresponding band gaps (B).

composites and pure TiO_2 were adversely decreased after sintering as a result of crystallization [10,12,41]. Fig. 6 shows the nitrogen gas adsorption–desorption isotherms and their respective pore size distribution (PSD) of the representative samples. The nitrogen gas adsorption–desorption isotherms of kaolinite, pure TiO_2, raw and composites calcined at 600 °C are presented in Fig. 6A. Pure kaolinite exhibited an isotherm with a sharp adsorbent uptake near $P/P_o = 1$ signifying the presence of macropores. On the other hand, pure TiO_2, as-synthesized and calcined samples of K-TiO_2 possess type IV isotherms depicting the presence of a mesoporous structure [28,41,42]. Indeed, their hysteresis loops are centered at relative pressures of $0.32 < P/P_o < 0.85$ representing the absence of macropores.

A close assessment of the hysteresis loops of the TT00 sample reveals the appearance of a triangular shape that can be categorized as Type H2 according to the IUPAC classification systems. The KT18, KT48 and their respective calcined samples (KT18-600 and KT48-600 as representative samples) also exhibited type H2 hysteresis loops. Generally, type H2 portrays the presence of aggregates with uniform channel-like pores [10,11,14,31]. The composites had smaller pore volumes than that of the TT00 sample but their pore sizes were essentially larger than that of pure TiO_2 (Table 3). The PSD of the samples obtained via this

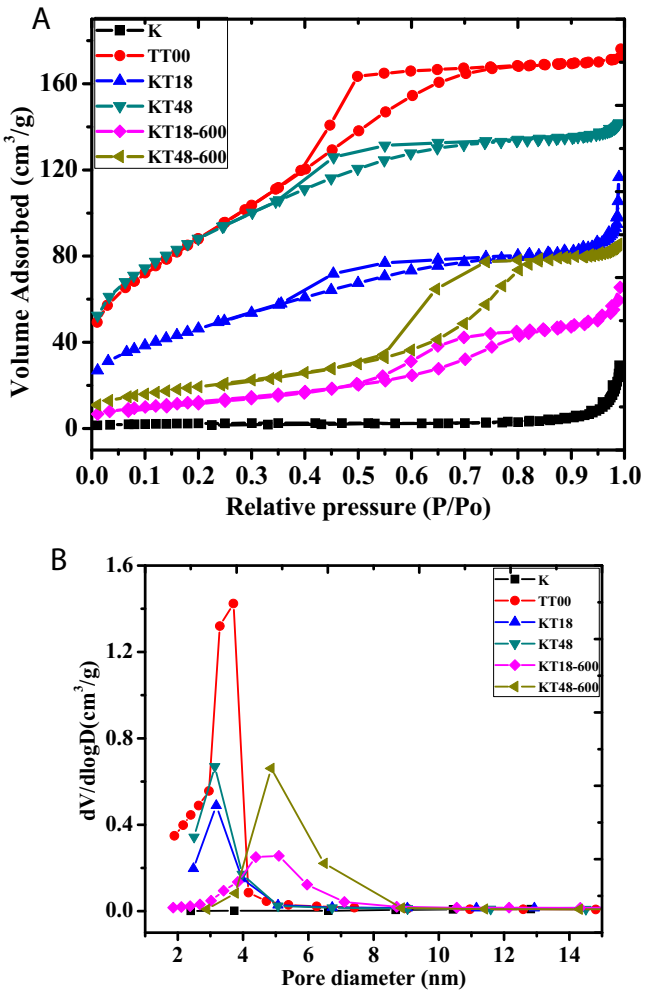


Fig. 6. Nitrogen gas adsorption–desorption isotherms of pure TiO_2, as-prepared K-TiO_2 and samples calcined at 600 °C as representative samples (A) and their respective PSD (B).

synthetic approach are compiled in Fig. 6B. It can be noted that all samples (except pure K) displayed similar patterns of PSD but with different average pore diameters. The as-synthesized samples displayed narrow pore distribution between 2 nm and 4.5 nm while the calcined samples had broad distribution ranging from ~3 to ~7 nm. The BET surface areas exhibited by the K-TiO_2 composites are superior to those reported in literature [14,27]. Thus, the porous structure and BET surface areas exhibited by the composites obtained in the present study indicate that the samples might be suitable for heterogeneous catalysis.

3.5. Morphology and microstructure of the photocatalysts

During sol–gel synthesis of materials, hydrolysis and condensation processes occur. It is therefore necessary to evaluate the appropriate pH conditions suitable for the formation of the final product with desirable properties for various applications. The pH of the reaction has a profound effect on the phase structure and morphology of the final product [43]. The morphology of the samples obtained in the present study was studied by SEM and TEM analyses. The SEM images of the KT2 and KT4 series obtained at different conditions are presented in Fig. 7 as representative samples of the K-TiO_2 composites. The morphological difference exhibited by the samples upon varying the TiO_2 content and pH can be noticed. Initially, the morphology of the pure kaolinite revealed the presence of plate-like structures. However, upon reaction with TiO_2 sol at different pH the kaolinite structures were essentially reduced to smaller particles containing spherical aggregates of TiO_2. Fig. 7A–B compares the microstructure of the KT24-600 and KT28-600 samples while Fig. 7C–D shows the images of the KT44-600 and KT48-600 samples, respectively (samples with higher TiO_2 loadings). At low pH the interaction between TiO_2 and kaolinite was enhanced leading to the formation of composites with well distributed particles (Fig. 7A and C). In the KT44-600 sample, the TiO_2 nanoparticles appear to grow on the edge of the kaolinite particles.

For the samples obtained at high pH (Fig. 7B and D), some of the plate-like kaolinite structures were retained with the TiO_2 being deposited on the surface. Further increase of the TiO_2 content leads to the stacking of the TiO_2 aggregates (Fig. 7D). This indicates that the formation of homogeneous photocatalysts can be achieved at low pH. Fig. 8 shows the X-ray mapping images and EDAX spectrum of the KT34-600 sample. X-ray mapping images portray that the elements were well distributed which is the necessary criterion for a photocatalyst suitable for heterogeneous catalysis. Moreover, the EDAX spectrum of this sample demonstrates that the composite consisted of Ti, Si, Al, O and K.

Fig. 9A presents the TEM images of the KT44-600 and KT48-600 samples. It can be seen that the photocatalysts consist of small particles less than 35 nm. The grain size observed from TEM analysis is very close to the grain size estimated by XRD (Table 1). The high-resolution TEM images of these samples reveal the presence of particles with a well-developed crystalline structure as a result of crystallization (Fig. 9B and D). Another notable feature is the aggregation behavior of the sample synthesized at pH 8 compared to the sample obtained at pH 4. It can be seen that the particles of the samples obtained at pH 8 were more aggregated than the grain obtained at pH 4. SEM image (Fig. 7D) revealed that the aggregation of the KT48-600 particles was brought about by the stacking of the TiO_2 nanoparticles. The crystalline structure, the formation of a Ti-rich composites and homogeneous distribution of the particles will presumably improve the photocatalytic properties of the composites obtained via this process.

3.6. Thermal analysis

K-TiO_2 composites with white fine particles, thermally stable, chemically inert at pH of 4–9 and non-toxic are suitable for photodegradation of organic pollutants and bacterial photodisinfection in the water treatment process; filler in the paper industry and UV filters [9,20,21,35,44,45]. The effect of the heat treatment in the KT18, KT48 and pure kaolinite samples was studied by the TGA-DTA analyses and the results are essentially presented in Fig. 10. The TGA curve of pure kaolinite shows a negligible weight loss in the temperatures <480 °C. Abrupt weight loss occurs at temperatures between 480 °C and 670 °C due to dehydroxylation of water in the silicate layers [22,27]. The endothermic peak centered at ~530 °C in the differential scanning calorimetric profile is ascribed to this process [46]. On the other hand, the composites displayed TG-DTA curves which are more or less different from that displayed pure kaolinite. Notable weight loss from the initial heating temperature to 230 °C is attributed to desorption of physisorbed water. Weight loss at 460–670 °C reveals the dehydroxylation of water in the silicate layers and crystallization of TiO_2 [13,27,32]. It was formerly reported [21,22] that sintering of the kaolinite at temperatures between 550 °C and 650 °C leads to the formation of metakaolin as the crystal structure of kaolinite breaks leaving an amorphous mixture of alumina and silica (Consider equation (1) below from reference [22]).

$$\underset{\text{Kaolinite}}{Si_2Al_2O_5(OH)_4} \xrightarrow[\Delta]{550-700\,^{\circ}C} \underset{\text{Metakaolin}}{Al_2O_3 \cdot 2SiO_2} + 2H_2O \quad (1)$$

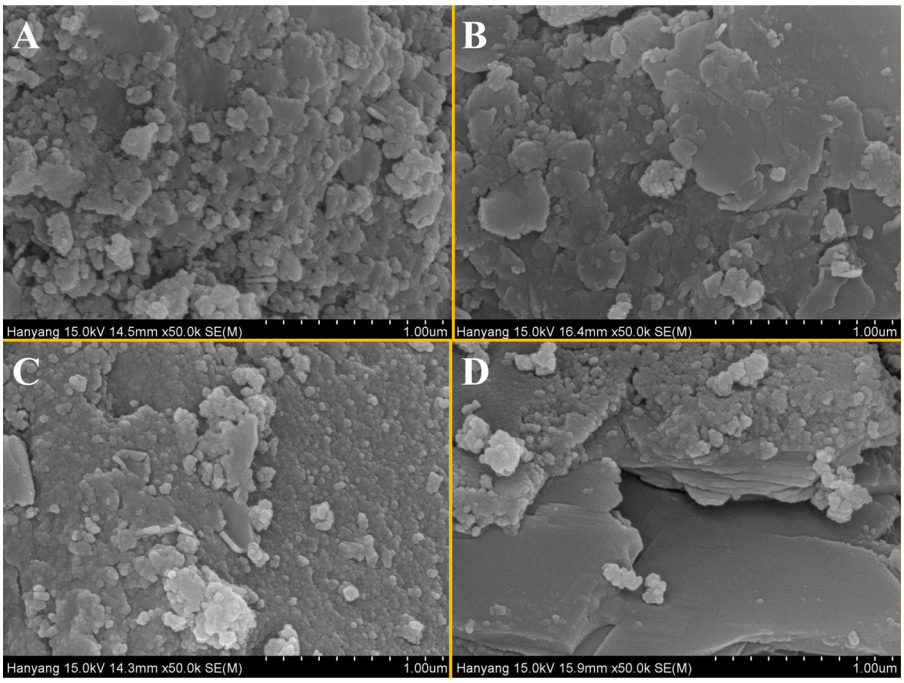


Fig. 7. SEM images of the K-TiO_2 photocatalysts obtained at different pH and calcined at 600 °C as representative samples; (A) KT24-600 (B) KT28-600 (C) KT44-600 (D) KT48-600.

In the presence of Ti–O– polymeric networks, Ti–O–Ti, Ti–O–Si, Si–O–Al and Si–O–Si can bridge through condensation of the –OH groups on the metal oxide networks [11,12,27]. The desorption of water and dehydroxylation processes are exquisitely substantiated by the appearance of a broad endothermic peak at 100 °C and 528 °C in the DTA curve, respectively. The broad exothermic peak that appears in the DTA curve at ~390 °C suggests the formation of TiO_2 crystals as a result of crystallization and interconnection of kaolinite with TiO_2 [27]. Additionally, the weight loss from the temperatures ≥600 °C is negligible indicating that a stable composite can be yielded through sintering at these particular temperatures. The TGA curves have shown that only ~15% of the composite was lost after heating the samples to 1000 °C. This signifies that the composites obtained in the present study are thermally stable hence different phases can be obtained through varying the sintering temperatures as was confirmed by the XRD results (Figs. 1–3).

3.7. Photocatalytic properties

The high surface area and porous structure displayed by the K-TiO_2 composites might influence the photocatalytic behavior of the samples as can substantially provide more adsorptive and photocatalytic active sites favorable for degradation of toxic organic

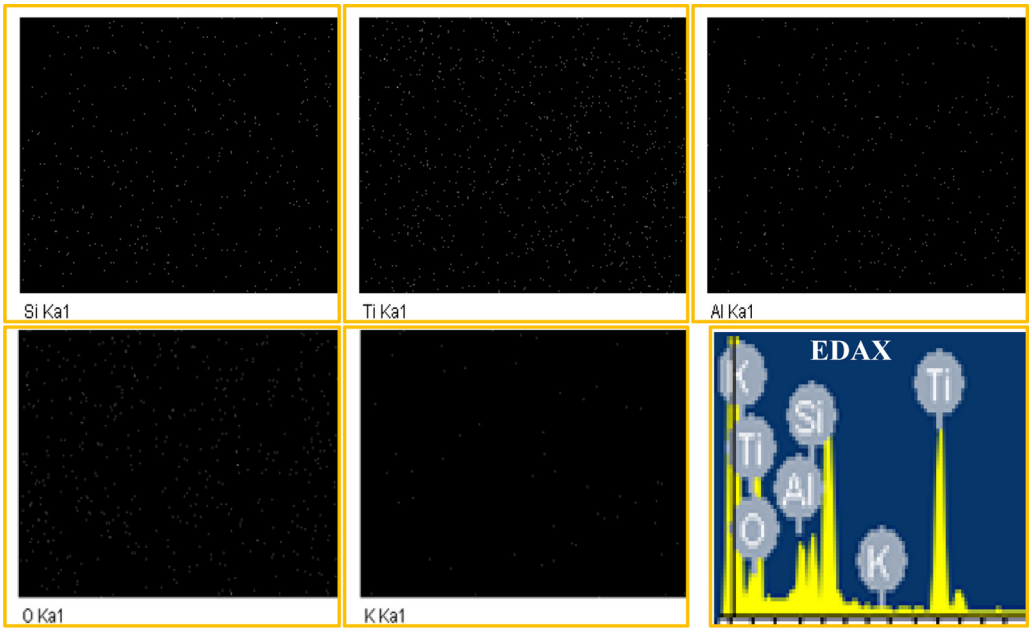


Fig. 8. X-ray mapping images and EDAX spectrum of the K-TiO_2 photocatalyst KT34-600 as a representative sample showing the presence and distributions of the elements.

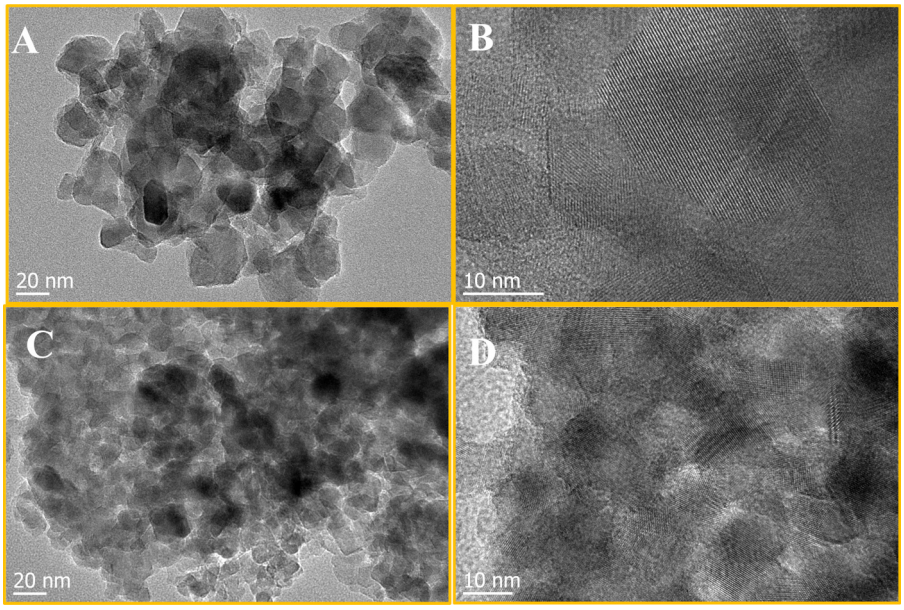


Fig. 9. Representative TEM images of the K-TiO_2 samples obtained at different conditions KT44-600 (A) KT48-600 (C); B and D are their respective high resolution TEM images.

pollutants [14,27]. The photocatalytic performance of the composites obtained in the present study was simply examined in the degradation of methylene blue solution in the presence of artificial UV light. A series of composites was obtained at pH 4 and 8 and then calcined at temperatures ranging from 400 °C to 900 °C. Preliminary photocatalytic experiments indicated that the samples obtained at pH 4 and calcined at 600 °C possessed better activities than those calcined at 400 °C and 900 °C and were also superior to the activities of the samples synthesized at pH 8 and calcined at different temperatures. Hence, only the activities of KT14-600, KT24-600, KT34-600 and KT44-600 will be discussed in this report and ultimately compared with photochemical performance of the ZrO_2-TiO_2 composites reported in our previous study [10].

Prior to actual irradiation, the adsorption–desorption behavior of the samples was examined. Fig. 11 displays the time dependent adsorption–desorption behavior of methylene blue solution.

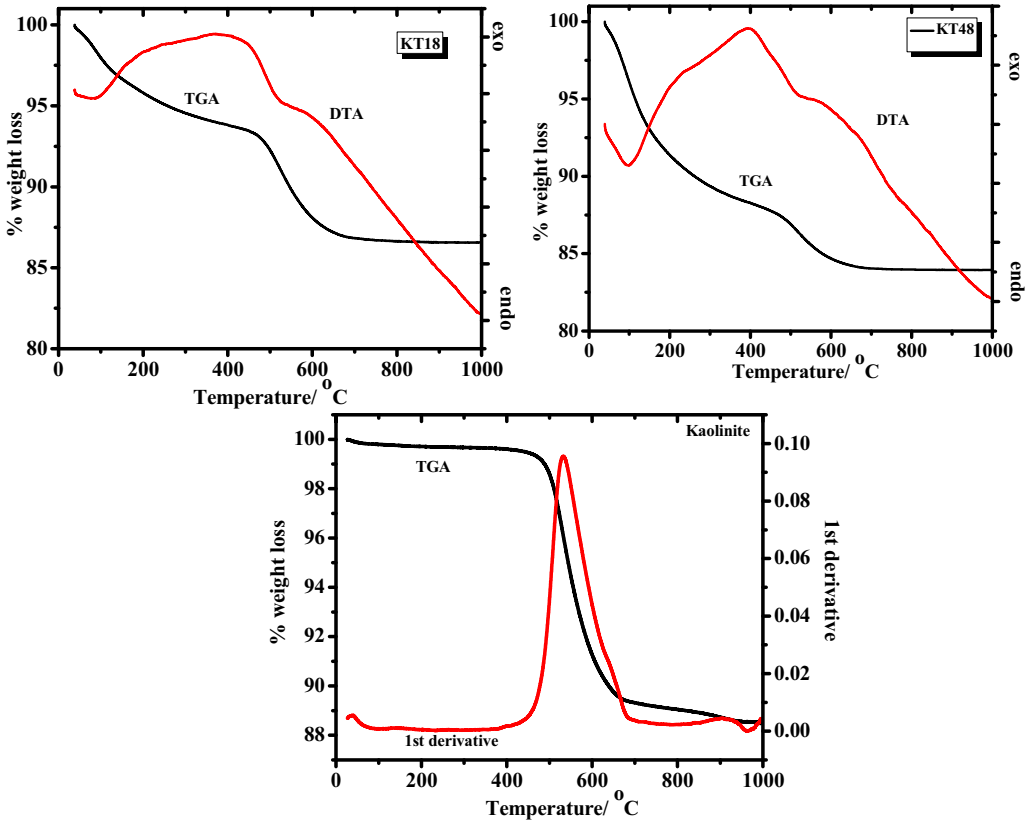


Fig. 10. TGA–DTA curves of pure kaolinite and the as-synthesized KT18 and KT48 samples.

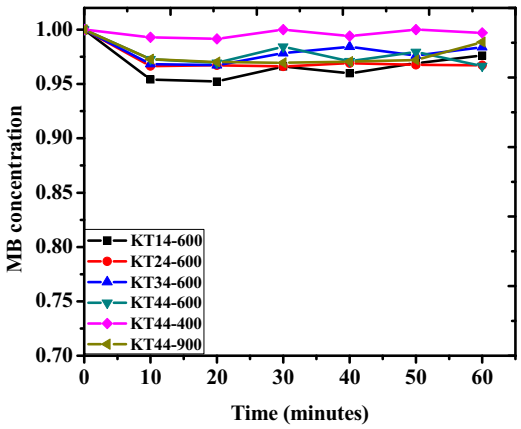


Fig. 11. Time dependent adsorption–desorption behavior of the photocatalysts before UV illumination.

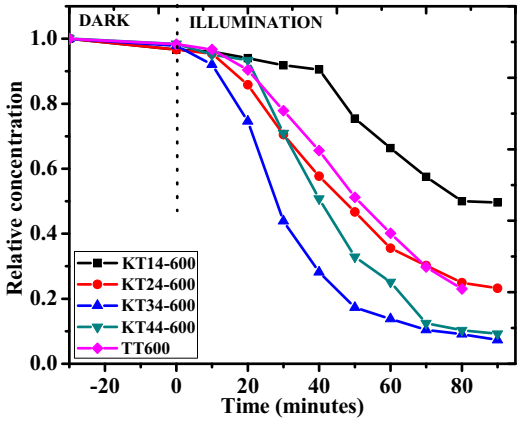


Fig. 12. Photocatalytic decolorization of MB solution by pure TiO_2 and K-TiO_2 photocatalysts calcined at 600 °C.

In the absence of UV light the amount up to 5% was adsorbed in the composites however, stirring the MB solutions for ≥20 min was enough to establish the adsorption–desorption equilibrium. Fig. 12 presents the photodecolorization of MB solution by the K-TiO_2 photocatalysts calcined at 600 °C under UV light illumination. The photocatalytic efficiency of the TT600 sample is included for the sake of comparison. It is noticeable that the used samples displayed different activities depending on their physicochemical properties such as TiO_2 content, calcination temperature, crystalline structure, crystallite size, surface area and porous structure. Using KT34-600 and KT44-600 samples, a photodecolorization efficiency ≥89% can be achieved within 70 min of irradiation. The KT34-600 exhibited the highest activity while the activity of the TT600 sample was higher than that of KT14-600. The photochemical performance of the samples appeared to obey the pseudo first-order reaction; thus the Langmuir–Hinshel–Wood model was used to estimate the rate constant of the photocatalysts [11,33,47]. Fig. 13 shows the linear correlation between the logarithms of relative concentration of MB solution ($\mathrm{Ln}\, C_o/C$) against the reaction time of the TiO_2 and K-TiO_2 samples calcined at 600 °C. From this plot it can be noticed that the rate constant of each of the samples is different implying that the performance depends on various physicochemical properties of materials. The rate constant of the KT34-600 sample was the largest while the KT14-600 sample was the lowest. Structural characterization of the composites revealed that Ti-rich photocatalysts with well-developed mixed phase structures and porous structure were produced after calcination at different calcination temperatures. The photocatalytic

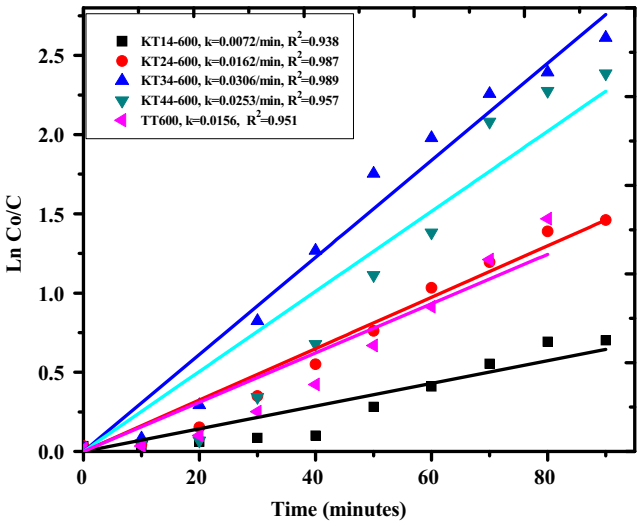


Fig. 13. Linear correlation between the logarithms of relative concentration of MB solution ($\mathrm{Ln}\, C_o/C$) against the reaction time of the TiO_2 and K-TiO_2 samples calcined at 600 °C.

performance of the samples obtained herein was largely influenced by the porous structure, amount of the TiO_2 in the composite, crystallinity, particle size and crystallite size.

The photocatalytic performance of the obtained samples was compared with the results obtained from our previous report using ZrO_2-TiO_2 photocatalysts [10]. In that particular report the photocatalytic performance of the ZrO_2-TiO_2 composites with different TiO_2 contents ranging from 30 to 60% was investigated in the decolorization of methylene blue. The sample with the 60% of TiO_2 (Zr/Ti = 0.8) registered the highest activity of all. In the present study, K-TiO_2 composites with the TiO_2 content ranging from ~40 to 90% were synthesized and the sample with the TiO_2 content of ~80% displayed the highest activity. In the present study we anticipated the samples with ~60% TiO_2 content to be the most active photocatalyst unfortunately, different results were obtained. A careful comparison of the rate constant of the samples with highest activities obtained in these two studies reveals that the rate constant of K-TiO_2 sample was 0.0306/min whereas that of the ZrO_2-TiO_2 with the Zr-to-Ti ratio of 0.8 was 0.0343/min. It can be seen that the rate constants of these photocatalysts are very close but it is notable that ZrO_2-TiO_2 was a better photocatalyst. In both cases, the photochemical properties of the obtained photocatalysts were improved as a result of the introduction of ZrO_2 and kaolinite, which improved the adsorptive capacity, porous structure and crystallinity of the materials to enhance their photochemical properties [14,48,49]. However, the possibility of synthesizing photoactive K-TiO_2 composites using convenient synthetic routes and precursors is interesting and recommendable.

4. Conclusions

In the present study, the effect of pH, TiO_2 content and calcination temperature on the crystalline structure, porosity and morphology of the kaolinite-titania composites was investigated. A versatile, economical and reproducible sol–gel route was used to synthesize K-TiO_2 samples with different TiO_2 content at pH 4 and 8 using titanium oxychloride as a TiO_2 source. The XRD, TGA and FTIR analyses revealed that kaolinite is incorporated in TiO_2 after thermal treatment and the calcination temperature ≥400 °C was sufficient to enhance the chemical interaction of the components. It was observed that TiO_2 crystals with a mixed phase (brookite and anatase) could be obtained in the samples synthesized at pH 4

and sintered at temperatures ≤600 °C while the mixture of anatase and brookite was absent in the calcined samples yielded at pH 8. A mixture of anatase and rutile was also observed in the samples calcined at ≤600 °C. The practical applicability of the samples was tested in the photodegradation of organic pollutants in the presence of UV light. It was observed that the KT34-600 exhibited the highest activity of all the composites synthesized via this route due to its superior properties. The effectiveness of these materials in degrading organic contaminants signifies that they can be alternative cheap photocatalysts suitable for degradation of dyes that are common pollutants in textile industries. Indeed, this experiment provides a criterion for selection of the appropriate synthetic conditions necessary for synthesis of the K-TiO_2 composites with suitable properties for various applications.

Acknowledgment

We are thankful to the Ministry of Trade, Industry and Energy of Korea for supporting this work (Grant No. 20124030200130) through the Human Resources Development program of the Korea Institute of Energy Technology Evaluation and Planning (KETEP).

References

[1] A. Fujishima, X. Zhang, D.A. Tryk, TiO_2 photocatalysis and related surface phenomena, Surf. Sci. Rep. 63 (2008) 515–582.
[2] K. Nakata, A. Fujishima, TiO_2 photocatalysis: design and applications, J. Photochem. Photobiol. C: Photochem. Rev. 13 (2012) 169–189.
[3] A. Fujishima, T.N. Rao, D.A. Tryk, Titanium dioxide photocatalysis, J. Photochem. Photobiol. C: Photochem. Rev. 1 (2000) 1–21.
[4] A. Fujishima, X. Zhang, Titanium dioxide photocatalysis: present situation and future approaches, Comptes Rendus Chimie 9 (2006) 750–760.
[5] M.R. Hoffmann, S.T. Martin, W.Y. Choi, D.W. Bahnemann, Environmental Applications of Semiconductor Photocatalysis, 1995, pp. 69–96.
[6] K. Hashimoto, H. Irie, A. Fujishima, TiO2 photocatalysis: a historical overview and future prospects, Jpn. J. Appl. Phys. Regul. Pap. Short Notes Rev. Pap. 44 (2005) 8269.
[7] T. Jiang, L. Zhang, M. Ji, Q. Wang, Q. Zhao, X. Fu, H. Yin, Carbon nanotubes/TiO_2 nanotubes composite photocatalysts for efficient degradation of methyl orange dye, Particuology 11 (2013) 737–742.
[8] C. Liu, H. Yin, L. Shi, A. Wang, Y. Feng, L. Shen, Z. Wu, G. Wu, T. Jiang, Preparation of hollow titania spheres and their photocatalytic activity under visible light, J. Nanosci. Nanotechnol. 14 (2014) 7072–7078.
[9] M.N. Chong, B. Jin, C.W.K. Chow, C. Saint, Recent developments in photocatalytic water treatment technology: a review, Water Res. 44 (2010) 2997–3027.
[10] G.N. Shao, S.M. Imran, S.J. Jeon, M. Engole, N. Abbas, M. Salman Haider, S.J. Kang, H.T. Kim, Sol–gel synthesis of photoactive zirconia–titania from metal salts and investigation of their photocatalytic properties in the photodegradation of methylene blue, Powder Technol. 258 (2014) 99–109.
[11] G.N. Shao, Y. Kim, S.M. Imran, S.J. Jeon, P.B. Sarawade, A. Hilonga, J.-K. Kim, H.T. Kim, Enhancement of porosity of sodium silicate and titanium oxychloride based TiO_2-SiO_2 systems synthesized by sol–gel process and their photocatalytic activity, Microporous Mesoporous Mater. 179 (2013) 111–121.
[12] G.N. Shao, A. Hilonga, Y.N. Kim, J.-K. Kim, G. Elineema, D.V. Quang, S.J. Jeon, H.T. Kim, Peptization technique in the synthesis of titania–silica composites and their photocatalytic properties, Chem. Eng. J. 198–199 (2012) 122–129.
[13] A. Hilonga, J.-K. Kim, P.B. Sarawade, H.T. Kim, Titania–silica composites with less aggregated particles, Powder Technol. 196 (2009) 286–291.
[14] Y. Zhang, H. Gan, G. Zhang, A novel mixed-phase TiO_2/kaolinite composites and their photocatalytic activity for degradation of organic contaminants, Chem. Eng. J. 172 (2011) 936–943.
[15] M. Xing, D. Qi, J. Zhang, F. Chen, B. Tian, S. Bagwas, M. Anpo, Super-hydrophobic fluorination mesoporous MCF/TiO_2 composite as a high-performance photocatalyst, J. Catal. 294 (2012) 37–46.
[16] G. Wang, L. Xu, J. Zhang, T. Yin, D. Han, Enhanced photocatalytic activity of TiO_2 powders (P25) via calcination treatment, Int. J. Photoenergy 2012 (2012).
[17] H.B. Wu, H.H. Hng, X.W. Lou, Direct synthesis of anatase TiO_2 nanowires with enhanced photocatalytic activity, Adv. Mater. 24 (2012) 2567–2571.
[18] D. Reyes-Coronado, G. Rodriguez-Gattorno, M. Espinosa-Pesqueira, C. Cab, R. De Coss, G. Oskam, Phase-pure TiO_2 nanoparticles: anatase, brookite and rutile, Nanotechnology 19 (2008) 145605.
[19] M. Ouzzine, M. Lillo-Ródenas, A. Linares-Solano, Photocatalytic oxidation of propene in gas phase at low concentration by optimized TiO_2 nanoparticles, Appl. Catal. B: Environ. 134 (2013) 333–343.
[20] M. Castellano, A. Turturro, P. Riani, T. Montanari, E. Finocchio, G. Ramis, G. Busca, Bulk and surface properties of commercial kaolins, Appl. Clay Sci. 48 (2010) 446–454.
[21] H.H. Murray, J.E. Kogel, Engineered clay products for the paper industry, Appl. Clay Sci. 29 (2005) 199–206.
[22] E.B.G. Johnson, S.E. Arshad, Hydrothermally synthesized zeolites based on kaolinite: a review, Appl. Clay Sci. 97–98 (2014) 215–221.
[23] H. Ming, Modification of kaolinite by controlled hydrothermal deuteration – a DRIFT spectroscopic study, Clay Miner. 39 (2004) 349–362.
[24] S. Letaief, T. Diaco, W. Pell, S.I. Gorelsky, C. Detellier, Ionic conductivity of nanostructured hybrid materials designed from imidazolium ionic liquids and kaolinite, Chem. Mater. 20 (2008) 7136–7142.
[25] J. Tokarský, P.J. Čapková, Burda, structure and stability of kaolinite/TiO_2 nanocomposite: DFT and MM computations, J. Mol. Model 18 (2012) 2689–2698.
[26] Z. Lu, M. Ren, H. Yin, A. Wang, C. Ge, Y. Zhang, L. Yu, T. Jiang, Preparation of nanosized anatase TiO_2-coated kaolin composites and their pigmentary properties, Powder Technol. 196 (2009) 122–125.
[27] K. Mamulová Kutláková, J. Tokarský, P. Kovář, S. Vojtěšková, A. Kovářová, B. Smetana, J. Kukutschová, P. Čapková, V. Matějka, Preparation and characterization of photoactive composite kaolinite/TiO_2, J. Hazard. Mater. 188 (2011) 212–220.
[28] G.N. Shao, A. Hilonga, S.J. Jeon, J.E. Lee, G. Elineema, D.V. Quang, J.-K. Kim, H.T. Kim, Influence of titania content on the mesostructure of titania–silica composites and their photocatalytic activity, Powder Technol. 233 (2013) 123–130.
[29] Y.N. Kim, G.N. Shao, S.J. Jeon, S.M. Imran, P.B. Sarawade, H.T. Kim, Sol–gel synthesis of sodium silicate and titanium oxychloride based TiO_2–SiO_2 aerogels and their photocatalytic property under UV irradiation, Chem. Eng. J. 231 (2013) 502–511.
[30] G.N. Shao, R. Sheikh, A. Hilonga, J.E. Lee, Y.-H. Park, H.T. Kim, Biodiesel production by sulfated mesoporous titania–silica catalysts synthesized by the sol–gel process from less expensive precursors, Chem. Eng. J. 215–216 (2013) 600–607.
[31] A. Hilonga, J.-K. Kim, P. Sarawade, H. Kim, Mesoporous titania–silica composite from sodium silicate and titanium oxychloride. Part I: grafting method, J. Mater. Sci. 45 (2010) 1255–1263.
[32] G.N. Shao, G. Elineema, D.V. Quang, Y.N. Kim, Y.H. Shim, A. Hilonga, J.-K. Kim, H.T. Kim, Two step synthesis of a mesoporous titania–silica composite from titanium oxychloride and sodium silicate, Powder Technol. 217 (2012) 489–496.
[33] W.S. Kuo, P.H. Ho, Solar photocatalytic decolorization of methylene blue in water, Chemosphere 45 (2001) 77–83.
[34] S. Tanemura, L. Miao, P. Jin, K. Kaneko, A. Terai, N. Nabatova-Gabain, Optical properties of polycrystalline and epitaxial anatase and rutile TiO_2 thin films by rf magnetron sputtering, Appl. Surf. Sci. 212–213 (2003) 654–660.
[35] C. Wang, H. Shi, P. Zhang, Y. Li, Synthesis and characterization of kaolinite/TiO_2 nano-photocatalysts, Appl. Clay Sci. 53 (2011) 646–649.
[36] S. Cassaignon, M. Koelsch, J.-P. Jolivet, Selective synthesis of brookite, anatase and rutile nanoparticles: thermolysis of $TiCl_4$ in aqueous nitric acid, J. Mater. Sci. 42 (2007) 6689–6695.
[37] A. Di Paola, G. Cufalo, M. Addamo, M. Bellardita, R. Campostrini, M. Ischia, R. Ceccato, L. Palmisano, Photocatalytic activity of nanocrystalline TiO_2 (brookite, rutile and brookite-based) powders prepared by thermohydrolysis of $TiCl_4$ in aqueous chloride solutions, Colloids Surf. A: Physicochem. Eng. Aspects 317 (2008) 366–376.
[38] J. Lee, Y. Yang, Estimation of reaction conditions for synthesis of nanosized brookite-type titanium dioxide from aqueous $TiOCl_2$ solution, J. Mater. Sci. 40 (2005) 2843–2847.
[39] M. Stir, R. Nicula, C. Bähtz, M. Knapp, E. Burkel, Phase Stability and Sintering Behaviour of Brookite-Free Nanostructured TiO2 Powders, 2015.
[40] H. Rahier, B. Wullaert, B. Van Mele, Influence of the degree of dehydroxylation of kaolinite on the properties of aluminosilicate glasses, J. Therm. Anal. Calorim. 62 (2000) 417–427.
[41] A. Nilchi, S. Janitabar-Darzi, A.R. Mahjoub, S. Rasouli-Garmarodi, New TiO_2/SiO_2 nanocomposites – phase transformations and photocatalytic studies, Colloids Surf. A: Physicochem. Eng. Aspects 361 (2010) 25–30.
[42] N. Yao, S. Cao, K.L. Yeung, Mesoporous TiO_2–SiO_2 aerogels with hierarchal pore structures, Microporous Mesoporous Mater. 117 (2009) 570–579.
[43] J. Sun, L. Gao, pH effect on titania-phase transformation of precipitates from titanium tetrachloride solutions, J. Am. Ceram. Soc. 85 (2002) 2382–2384.
[44] H.H. Murray, Chapter 5 kaolin applications, in: H.M. Haydn (Ed.), Developments in Clay Science, Elsevier, 2006, pp. 85–109.
[45] M.N. Chong, B. Jin, C.P. Saint, Bacterial inactivation kinetics of a photodisinfection system using novel titania-impregnated kaolinite photocatalyst, Chem. Eng. J. 171 (2011) 16–23.
[46] L.C. Edomwonyi-Otu, B.O. Aderemi, A.S. Ahmed, N.J. Coville, M. Maaza, Influence of thermal treatment on Kankara kaolinite, Opticon1826 5 (2013) 1–5.
[47] A. López, D. Acosta, A.I. Martínez, J. Santiago, Nanostructured low crystallized titanium dioxide thin films with good photocatalytic activity, Powder Technol. 202 (2010) 111–117.
[48] J.H. Schattka, D.G. Shchukin, J. Jia, M. Antonietti, R.A. Caruso, Photocatalytic activities of porous titania and titania/zirconia structures formed by using a polymer gel templating technique, Chem. Mater. 14 (2002) 5103–5108.
[49] S.Y. Murakami, H. Kominami, Y. Kera, S. Ikeda, H. Noguchi, K. Uosaki, B. Ohtani, Evaluation of electron-hole recombination properties of titanium (IV) oxide particles with high photocatalytic activity, Res. Chem. Intermed. 33 (2007) 285–296.